Hydrogen bond breaking probed with multidimensional stimulated vibrational echo correlation spectroscopy

John B. Asbury, Tobias Steinel, C. Stromberg, K. J. Gaffney, I. R. Piletic, and M. D. Fayer
Department of Chemistry, Stanford University, Stanford, California 94305

(Received 8 April 2003; accepted 29 September 2003)

Hydrogen bond population dynamics are extricated with exceptional detail using ultrafast (<50 fs) infrared multidimensional stimulated vibrational echo correlation spectroscopy with full phase information and frequency resolved infrared pump–probe experiments performed on the hydroxyl stretch of methanol–OD oligomers in CCl_4. Hydrogen bond breaking makes it possible to acquire data for times much greater than the hydroxyl stretch vibrational lifetime. The correlation spectra and detailed calculations demonstrate that vibrational relaxation leads to hydrogen bond breaking for oligomers that have hydroxyl stretch frequencies on the low energy (red) side of the hydroxyl stretch spectrum, the spectral region that is associated with the strongest hydrogen bonds. Frequency resolved pump–probe data support the conclusions drawn from the correlation spectra. Using a global fit to the pump–probe spectra, in conjunction with assignments made possible through the correlation spectra, it is demonstrated that the residual ground state and photoproduct of hydrogen bond breaking are prepared near their thermal equilibrium distribution. The spectrum of the hydrogen bond breaking photoproduct and the residual ground state approach the steady-state temperature difference spectrum on the tens of picoseconds time scale, indicating the system thermalizes on this time scale. © *2003 American Institute of Physics.* [DOI: 10.1063/1.1627762]

I. INTRODUCTION

Hydrogen bonding in alcohol liquids and water gives rise to complex structures and dynamics. In hydrogen bonding liquids, hydrogen bonds are constantly being broken and formed.[1] The structural dynamics of hydrogen bond networks play an important role in determining the properties of hydrogen bonding liquids. Such liquids have generated a great deal of experimental[2–20] and theoretical[21–28] study because of their importance as solvents in chemical and biological systems. Recently, applications of ultrafast infrared spectroscopic experiments are producing increased understanding of hydrogen bond dynamics. While most ultrafast infrared experiments have utilized pump–probe spectroscopy,[5–16] development of the ultrafast infrared vibrational echo technique[29–32] and the recent extension to multidimensional vibrational echo methods,[33–35] provide a new approach for the study of hydrogen bond dynamics. Multidimensional techniques are beginning to be applied to hydrogen bonding systems.[18–20] Multidimensional stimulated vibrational echo methods are closely related to multidimensional NMR experiments.[36–38] However, multidimensional stimulated vibrational echo correlation spectroscopy operates on a sufficiently fast time scale (tens of fs) to directly examine the time evolution of hydrogen bonding networks.

Examination of the hydroxyl stretch provides information on hydrogen bonding because the frequency of the hydroxyl stretch is sensitive to the strength and type of hydrogen bonding.[1,39,40] Fluctuations in the populations and strengths of hydrogen bonds produce hydroxyl stretch spectral evolution.[8,21,41] The linear absorption spectrum cannot be used to examine spectral evolution because absorption lines in hydrogen bonded liquids are inhomogeneously broadened[3,4,8,11,19,20,22,42] and yield only time independent information. The inhomogeneous contribution to the line shape can be eliminated and the underlying dynamical line shapes can be observed using vibrational echo experiments.[29–35,43] Because of the complexity of hydrogen bonding systems, analysis of different contributions to dynamical vibrational spectra requires ultrafast multidimensional methods. Such methods can separate and narrow the dynamic spectral features,[29–35,43] permitting the observation of various contributions to the dynamics.

In this paper, multidimensional stimulated vibrational echo correlation spectroscopy with full phase information is applied to the study of methanol–OD (MeOD) oligomers in CCl_4. Figure 1 is a spectrum of 10% MeOD in CCl_4 with a schematic illustration of the different types of hydrogen bonding species. For a MeOD in an oligomer in which the OD is both a hydrogen bond donor and acceptor (called δ), the OD stretch is centered at $\sim 2490\ \mathrm{cm}^{-1}$, and it has a FWHM of $\sim 150\ \mathrm{cm}^{-1}$. An OD that is a hydrogen bond donor but not an acceptor (called γ) has a peak position of $\sim 2600\ \mathrm{cm}^{-1}$ and a FWHM of $\sim 80\ \mathrm{cm}^{-1}$. An OD that is an acceptor but not a donor (called β) has a spectrum centered at $2690\ \mathrm{cm}^{-1}$ with a $20\ \mathrm{cm}^{-1}$ FWHM.[6] The shift to the lower energy and the broad spectra of the δ and γ bands are caused by the change in the hydroxyl stretch potential with hydrogen bonding.[1,39,40] The high energy (blue) side of the δ band is associated with weaker hydrogen bonds and the low energy (red) side results from stronger hydrogen bonds.[1,39,40,44] Breaking a hydrogen bond changes the nature

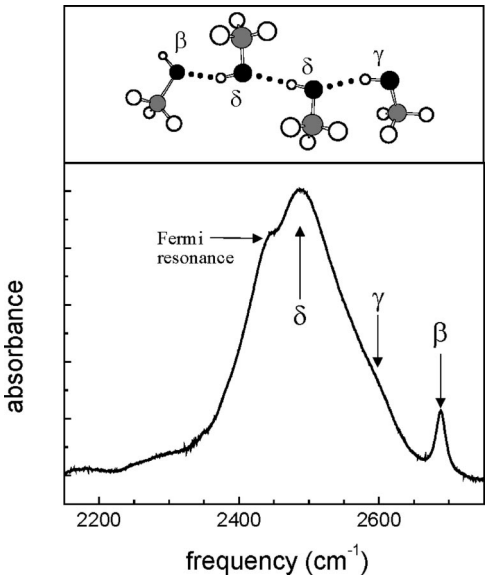

FIG. 1. The linear absorption spectrum of a 10% solution of methanol–OD in CCl_4. β's are hydroxyls that are acceptors but not donors. γ's are donors but not acceptors. δ's are both donors and acceptors. These are illustrated schematically at the top of the figure. The shoulder on the red side of the spectrum is a Fermi resonance with the overtone of the methyl rocking mode. This feature is absent in fully deuterated methanol.

of the species and, therefore, its absorption frequency. In an oligomer longer than a trimer, if a δ breaks a hydrogen bond, two δ absorbers are lost from the absorption spectrum, and a γ and a β are formed (see schematic in Fig. 1).[6] Therefore, the dynamics of the spectrum of the hydroxyl stretch reflect the population dynamics of the hydrogen bonds. The time dependent shapes and positions of the bands in the vibrational echo correlation spectra provide information on the structural evolution of the system. Initial experiments using multidimensional vibrational echoes to study MeOD oligomers have been presented.[3,4]

Recently, vibrational relaxation and hydrogen bond dynamics in MeOD dissolved in CCl_4 were measured with ultrafast infrared pump–probe spectroscopy.[5–8] The hydroxyl stretch of δ MeODs was excited at 2500 cm^{-1}. Following vibrational relaxation with a $\sim$500 fs lifetime, the signal did not decay to zero because of hydrogen bond breaking that preserved the ground state bleach in the δ band. The studies showed that hydrogen bond breaking occurred following vibrational relaxation on two time scales, $\sim$200 fs and $\sim$2 ps.[6] The fast rate arises from a direct breaking mechanism wherein the excited hydroxyl stretch decays into vibrational modes that directly lead to the hydrogen bond dissociation. The slower rate of breaking is caused by an indirect mechanism wherein the dissociation of hydrogen bonds follows vibrational energy flow from the initially excited molecule to other MeODs of the same oligomer.[6] The pump–probe signal does not decay monotonically to zero. Rather, following a rapid decay the signal increases to a second maximum at $\sim$4 ps because of the hydrogen bond breaking. The decay from the second maximum, caused by hydrogen bond reformation, occurs on two time scales, with $\sim$7 and $\sim$20 ps time constants. The excited state lifetime was found to be wavelength dependent, varying from $\sim$900 fs at 2550 cm^{-1} to $\sim$400 fs at 2450 cm^{-1}.[6]

Here, we present an expanded experimental study of vibrational relaxation and hydrogen bond dynamics in MeOD and *d*-MeOD (fully deuterated methanol) dissolved in CCl_4 using the shortest mid-IR pulses produced to date ($<$50 fs or $<$4 cycles of light). Because of the very large bandwidth associated with the ultrashort pulses, it is possible to perform experiments on the entire broad hydroxyl stretching 0–1 and 1–2 bands of MeOD oligomers even though the combined ground state and first excited state bands of MeOD are $\sim$400 cm^{-1} wide. We begin by discussing frequency resolved IR pump–probe spectra of *d*-MeOD. In contrast to MeOD, the excited state lifetime is wavelength independent across the broad hydroxyl stretch band because a Fermi resonance with the overtone of the methyl rocking mode (shoulder on the red side of the spectrum in Fig. 1) is absent in *d*-MeOD.[3,4] Consequently, we are able to employ a global fitting procedure in both time and frequency that incorporates the detailed kinetic model developed previously to explicate the hydrogen bond dynamics.

To obtain information beyond that available from the linear absorption spectrum and spectrally resolved pump–probe experiments, a detailed report is presented of the first application of ultrafast heterodyne detected multidimensional stimulated vibrational echo correlation spectroscopy with full phase control to the study of the dynamics of hydrogen bonding liquids.[3,4] The resulting correlation spectra include both the 0–1 and 1–2 vibrational transitions. By using pulses that are transform limited in the sample and by controlling path lengths with accuracy of a small fraction of a wavelength of light along with proper data analysis, correlation spectra are obtained with correct phase relationships across the entire spectrum in a manner that is similar to 2D NMR spectroscopy.[36–38] The correlation spectra contain information that is not available from other spectroscopic probes of vibrational relaxation and hydrogen bond dynamics.

The vibrational echo correlation spectroscopy technique measures the population and vibrational dephasing dynamics in two frequency dimensions, ω_m and ω_τ. The ω_m axis is similar to the frequency axis in frequency resolved pump-probe spectroscopy. Hydrogen bond dynamics represent a photochemical system in which vibrational excitation of the hydroxyl stretch results in hydrogen bond breaking.[5,6,8,45] Therefore, the ω_m axis provides information on the identity of the species that result from hydrogen bond breaking. The ω_τ axis does not have an analog in the pump–probe experiment; it provides an additional dimension of information that is contained only in the correlation spectrum. The positions and signs of peaks in the correlation spectra contain the history of the various species involved in the hydrogen bonding dynamics. Separation of the peaks in the two-dimensional (2D) correlation spectrum is equivalent to separation of quantum pathways even though the pathways result in optical emission at the same frequency. Interferences between peaks with different histories are removed, which simplifies the interpretation of the sequence of events.[3,4] The correlation spectra and comparison to detailed calculations unambiguously demonstrate that hydrogen bonds are broken selec-

tively on the red side of the δ band and that the photoproduct of hydrogen bond breaking, γ MeODs, are created.

II. EXPERIMENTAL PROCEDURES

The ultrashort IR pulses are generated using a Ti:sapphire regeneratively amplified laser/OPA system. The output of the regen is 26 fs transform limited 2/3 mJ pulses at 1 kHz rep rate. These are used to pump a substantially modified Spectra Physics short pulse IR OPA. The output of the OPA is compressed to produce <50 fs virtually transform limited IR pulses as measured by collinear autocorrelation. For the experiments, the compression was readjusted to give transform limited pulses in the sample as measured by a sample that gave a purely nonresonant signal. The long-term stability is such that data were collected continuously for as long as five days.

For the heterodyne detected multidimensional stimulated vibrational echoes, the IR beam is split into five beams. Three of the beams are the excitation beams for the stimulated vibrational echo. A fourth beam is the local oscillator (LO) used to heterodyne detect the vibrational echo signal. All of the beams that pass through the sample are optically identical and are compensated for GVD simultaneously. The vibrational echo signal combined with the LO is passed through a monochromator. For the spectrally resolved pump–probe experiments, one of the excitation beams is used for pump–probe experiments. The fifth beam is ten times weaker than the others and is used as the probe beam. After passing through the sample, the probe beam is directed into the monochromator. Depending on the experiment, the heterodyne detected echo or the probe beam is detected by a 32 element MCT array. At each monochromator setting, the array detects 32 individual wavelengths. The data were processed using a computer that acted as a digital lock-in amplifier that was synchronized to an optical chopper.

Difference intensity measurements were made for both the vibrational echo and pump–probe experiments. For the first laser pulse, the array measured the local oscillator or probe beam and the corresponding signal field. For the next laser shot, the optical chopper blocked one of the beams to prevent the signal field from being generated and only the local oscillator or probe beam was measured. The difference between these two measurements was then normalized by the spectrum of the local oscillator or probe detected in the second shot to remove the effect of pixel-to-pixel variations in the array. Both the heterodyne detected vibrational echo and the pump–probe signal are quadratic in the intensity of the laser. A single element detector measured the overall intensity of the laser, and was used to do a second normalization of the signals to provide the proper quadratic normalization.

The sample, 10% MeOD or 10% *d*-MeOD in CCl_4, was held in a sample cell of CaF_2 flats with a spacing of 50 μm. The peak absorbance of the samples was 0.18. Such a low absorbance is necessary to prevent serious distortions of the pulses as they propagate through the sample.

For the spectrally resolved pump–probe experiments, the change in transmission spectrum was collected as a function of the delay between the pump and probe pulses. The monochromator was stepped across the spectrum so that the arrays of wavelengths measured by the different array blocks matched up to form a continuous spectrum across the entire hydroxyl stretch band. The pump pulse was delayed in variable steps. The spectrum of the pump and probe pulses were identical. The spectrum of the probe was removed from the data as the data were collected. The data were not corrected for the spectrum of the pump; it is sufficiently broad to span the desired spectral region.

The phase-resolved, heterodyne detected, stimulated vibrational echo was measured as a function of one frequency variable, ω_m, and two time variables, τ and T_w, which are defined as the time between the first and second radiation field-matter interactions and the second and third interactions, respectively. The measured signal is the absolute value squared of the sum of the vibrational echo electric field, S, and the local oscillator electric field, L: $|L+S|^2=L^2+2LS+S^2$. The L^2 term is time-independent and the S^2 is negligibly small; hence, neither contributes to the time dependence of the signal. The spectrum of the $2LS$ term is the ω_m frequency axis. As the τ variable is scanned in 2 fs steps, the phase of the echo electric field is scanned relative to the fixed local oscillator electric field, resulting in an interferogram measured as a function of the τ variable. The interferogram contains the amplitude, sign, frequency, and phase of the echo electric field as it varies with τ. By numerical Fourier transformation, this interferogram is converted into the frequency variable ω_τ. In NMR, the ω_τ and the ω_m axes are generally referred to as the ω_1 and the ω_3 axes, respectively.

The interferogram contains both the absorptive and dispersive components of the vibrational echo signal. However, two sets of quantum pathways can be measured independently by appropriate time ordering of the pulses in the experiment.[37,38] With pulses 1 and 2 at the time origin, pathway 1 or 2 is obtained by scanning pulse 1 or 2 to negative time, respectively. In principle, by adding the Fourier transforms of the interferograms from the two pathways, the dispersive component cancels leaving only the absorptive component.[4,37,38] The 2D vibrational echo correlation spectra are constructed by plotting the amplitude of the absorptive part of the stimulated vibrational echo as a function of both ω_m and ω_τ.

Lack of perfect knowledge of the timing of the pulses and consideration of chirp on the vibrational echo pulse requires a ''phasing'' procedure to be used.[4] The projection slice theorem[4,36–38] is employed to generate the absorptive 2D correlation spectrum. The projection of the absorptive 2D correlation spectrum onto the ω_m axis is equivalent to the IR pump–probe spectrum recorded at the same T_w, as long as all the contributions to the stimulated vibrational echo are absorptive. Consequently, comparison of the projected 2D stimulated vibrational echo spectrum with the pump–probe spectrum permits the correct isolation of the absorptive vibrational echo correlation spectrum from the 2D spectrum obtained from the addition of the two quantum pathways.

It is possible to come relatively close to the correct correlation spectrum prior to the ''phasing'' procedure because the very short pulses permit their time origins to be known

within a few fs. The frequency dependent phasing factor used to correct the 2D spectra has the form

$$S_C(\omega_m,\omega_\tau)=S_1(\omega_m,\omega_\tau)\Phi_1(\omega_m,\omega_\tau)+S_2(\omega_m,\omega_\tau)\Phi_2(\omega_m,\omega_\tau),$$

$$\Phi_1(\omega_m,\omega_\tau)=\exp[i(\omega_m\Delta\tau_{\mathrm{LO},E}+\omega_\tau\Delta\tau_{1,2}+Q\omega_m\omega_m+C\omega_m\omega_\tau)],$$

$$\Phi_2(\omega_m,\omega_\tau)=\exp[i(\omega_m\Delta\tau_{\mathrm{LO},E}-\omega_\tau\Delta\tau_{1,2}+Q\omega_m\omega_m+C\omega_m\omega_\tau)]. \quad (1)$$

Each term in Eq. (1) has a well-defined physical origin. S_C, is the correlation spectrum. S_1 and S_2 are the spectra recorded for pathways 1 and 2, respectively. $\Delta\tau_{\mathrm{LO},E}$ accounts for the lack of perfect knowledge of the time separation of the LO pulse and the vibrational echo pulse; the term involving Q accounts for linear chirp introduced into the echo pulse by the rear window of the sample cell; $\Delta\tau_{1,2}$ accounts for the lack of perfect knowledge of the time origins of excitation pulses 1 and 2; and the term involving C accounts for the linear chirp caused by propagation of the echo pulse through the sample. Following phasing, the errors are $<100\times10^{-18}$ s across the entire spectrum.

III. RESULTS AND DISCUSSION

A. Pump–probe spectra

Figure 2(a) shows pump–probe spectra of 10% *d*-MeOD in a frequency-time contour plot as a function of pump delay, t (note the log t scale). The color bar to the right keys the color of each contour to the corresponding amplitude. The contours display equal 8% graduations. *d*-MeOD rather than MeOD was studied because the δ and γ excited state lifetimes are wavelength independent due to the absence of a Fermi resonance between the hydroxyl stretch and the overtone of the methyl rocking mode.[4,46] The time dependence of the photoproduct spectra are more easily extracted without the complication of wavelength dependent excited state lifetimes during the first few ps. Other than the wavelength dependent lifetime, comparisons of experiments show that the dynamics of *d*-MeOD and MeOD are the same. Figure 2(b) displays a global fit to the pump–probe data that was employed to assign the different populations contributing to the dynamics. The fit will be discussed in detail below.

At pump delay $t=200$ fs [bottom of Fig. 2(a)], the spectrum is dominated on the blue side by the positive going 0–1 transition of the δ and γ bands and on the red side by the negative going 1–2 transition of the δ. The 1–2 transition of the γ band is obscured by the much larger positive 0–1 transition of the δ band. The γ 0–1 transition is centered at 2600 cm^{-1}. With an anharmonicity of ~100 cm^{-1},[47] the γ 1–2 transition is centered at ~2500 cm^{-1}, directly on top of the δ 0–1 transition. The relative intensity of the γ 0–1 and 1–2 transitions are much smaller compared with the δ 0–1 and 1–2 transitions because the concentration of the γ is lower,[5,6,26] the extinction coefficient is three times smaller,[48] and the laser spectrum at 2600 cm^{-1} is approximately 60% compared to its maximum at 2480 cm^{-1}. These combined

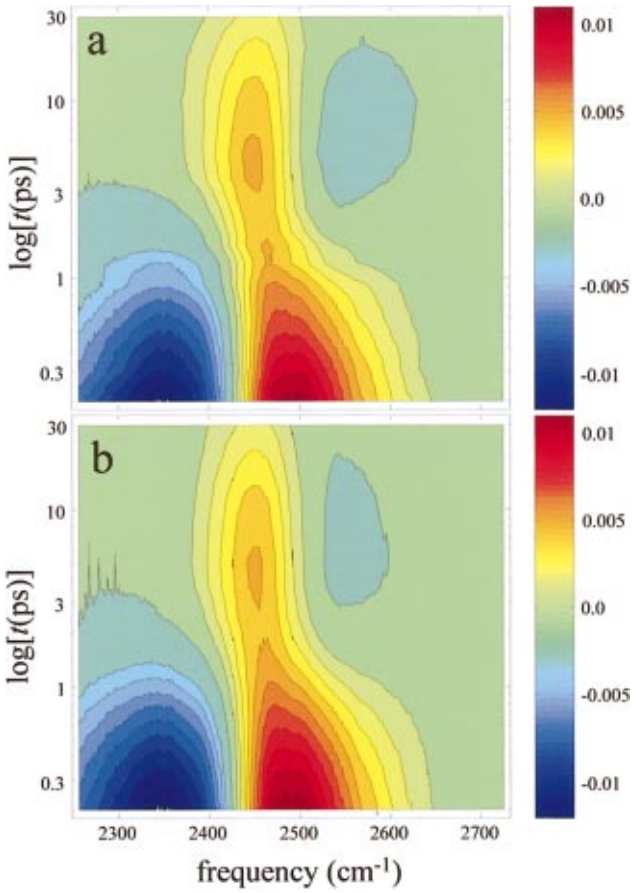

FIG. 2. (Color) (a) Frequency-time contour plots of spectrally resolved pump–probe data collected as a function of pump delay, t (note the log t scale). The z axis, shown as contours, has units of transmission change (arbitrary units). The positive going (red) features at small t are the 0–1 transitions of the initially excited δ and γ bands. The negative going (blue) features are the 1–2 transition of the δ band. At longer t, the positive going spectrum narrows and shifts to the red because of hydrogen bond breaking and a new negative going feature appears. The 1–2 band decays with the vibrational lifetime. (b) A global (frequency-time) fit of the pump–probe spectra using a previously reported kinetic model. The agreement is excellent. See text for details of the fitting procedure.

effects make the intensity of the γ 0–1 and 1–2 transitions ~20 times smaller than their δ band counterparts. The γ 0–1 transition appears in the pump–probe spectra as a small positive shoulder next to the large positive δ 0–1 transition. The γ 1–2 transition is not visible because it is a $\sim5\%$ negative cut-out of the center of the large δ 0–1 transition.

For $t\sim1$ ps, the negative going 1–2 transition of the δ band has decayed with the excited state lifetime and is nearly gone. The positive going 0–1 δ band appears to collapse to the red and narrow. By $t\sim4$ ps, the positive δ 0–1 band has finished moving to the red. The peak reaches another maximum because of continued hydrogen bond breaking.[6] Hydrogen bond breaking, which converts δ's into γ's and β's, prevents excited state relaxation from completely filling in the ground state bleach. Consequently, the δ band is preserved for times longer than the excited state lifetime through hydrogen bond breaking.[6] In addition, a new negative going feature appears to the blue of the preserved δ band. Although there is more than one mechanism that can give rise to the observed features in the pump–probe spectrum, it will be

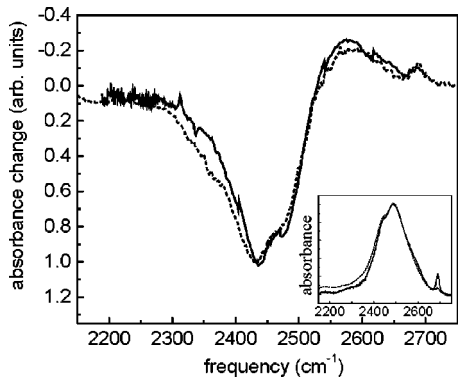

FIG. 3. Normalized comparison of $t=30$ ps pump–probe spectrum of 10 mol % MeOD in CCl_4 (solid line) with FTIR temperature difference spectrum of 26 mol % MeOD in CCl_4 (dashed line). The spectra are nearly identical. The corresponding linear FTIR spectra are shown in the inset. As can be seen from the inset, the small differences between the pump–probe spectrum and the temperature difference spectrum result from the differences in the samples.

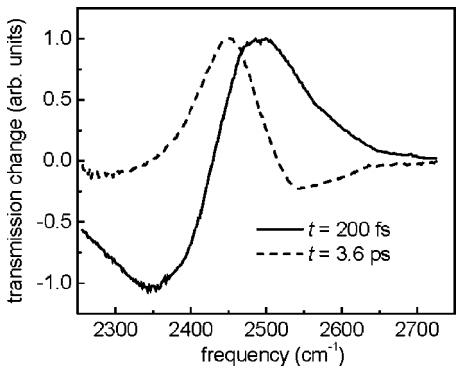

FIG. 4. Normalized comparison of spectral slices from the pump–probe data. The spectra at $t=200$ fs and 3.6 ps are shown to illustrate the dramatic change in the spectrum of the preserved δ band (positive) due to selective breaking of strong hydrogen bonds on the red side of the band.

shown conclusively below using correlation spectroscopy and detailed calculations that this band corresponds to the photoproduct γ produced by hydrogen bond breaking.[6] Therefore, we will discuss the data in terms of the correct mechanism prior to the elimination of other possible mechanisms. Finally, for $t>4$ ps, the amplitudes of the preserved δ and photoproduct γ spectra decay because of hydrogen bond recombination until a long time offset is observed, as reported previously.[6] The long term offset is produced by a very small increase in the sample temperature following vibrational relaxation that shifts the equilibrium to fewer hydrogen bonds.

To understand the vibrational relaxation and hydrogen bond dynamics observed in the pump–probe spectra, we start by assigning the species in the long t portion of the spectra. The long t portion of the spectra contains contributions only from the preserved δ and photoproduct γ bands. Figure 3 shows the comparison of the $t=30$ ps pump–probe spectrum of 10 mol % MeOD with the steady-state temperature difference spectrum of 26 mol % MeOD measured previously.[5,6] The temperature difference spectrum is for a 9 °C change in temperature and is a strictly steady-state experiment. When the temperature is raised, the distribution of hydrogen bonds shifts toward fewer hydrogen bonds and potentially weaker bonds. Because the hydroxyl stretch frequency depends on the strength of hydrogen bonds associated with it, a shift toward weaker hydrogen bonds would produce a blueshift in the spectrum. If hydrogen bonds were lost selectively from the red side of the spectrum, then the spectrum would also shift to the blue. In either case, a blueshift of the spectrum would occur. The shift toward the blue at higher temperature depletes the red side of the spectrum, which corresponds to stronger hydrogen bonds.

The $t=30$ ps spectrum closely matches the steady-state temperature difference spectrum indicating the distribution of hydrogen bonds in the sample has reached its thermally equilibrated distribution in ~ 30 ps. The small differences in the two spectra result from the different samples that were used. The FTIR spectra of the two samples at room temperature are shown in the inset of Fig. 3. The 26 mol % sample has slightly more absorbance on the red side of the δ band because, on average, the oligomers are longer.[26] The longer oligomers reduce the relative concentration of γ's, which makes the γ band (blue side of the line) smaller compared with the 10 mol % sample. The $t=30$ ps pump–probe spectrum reflects these differences.

Having assigned the preserved δ and photoproduct γ populations in the long t portion of the pump–probe spectra, we now turn to the earlier t regions to explore when the preserved δ and photoproduct γ populations were formed. As mentioned earlier, the δ and γ excited state lifetimes are the same in d-MeOD (0.8 ps) because of the absence of the Fermi resonance on the red side of the δ band that shortens the δ lifetime in MeOD.[4] Consequently, we are able to describe the spectra and dynamics of excited state decay with a single basis function, which decays exponentially with the excited state lifetime. At the earliest delays ($t \ll 1$ ps) the pump–probe spectra in Fig. 2(a) are dominated by the ground state bleach and excited state absorption and stimulated emission. Therefore, we chose the earliest pump–probe spectrum ($t=200$ fs) as a basis function ($B_1(\omega)$) to fit the excited state lifetime decay of *both* δ and γ bands. This spectrum is shown as the solid line in Fig. 4. To describe the frequency and time dependence of hydrogen bond breaking and reformation, we adopt a model which assumes the spectrum of the preserved δ and photoproduct γ bands are virtually time independent. This assumption allows us to select a pump–probe spectrum that displays only the preserved δ and photoproduct γ spectra and use it as a basis function to describe the spectrum of the species that have broken hydrogen bonds at all times, t. We selected the $t=3.6$ ps pump–probe spectrum as the second basis function ($B_2(\omega)$) to describe the preserved δ and photoproduct γ spectra because it is the earliest spectrum that contains no contribution from the excited states. This spectrum is shown as the dashed line in Fig. 4. (Note that Fig. 4 is the transmission change while Fig. 3 is the absorbance change.)

To apply this model to the pump–probe data, we employed a global fitting procedure to fit the data set in both time and frequency domains simultaneously. The frequency dependence was described by the basis functions introduced above. To describe the time dependence, we adopted the kinetic model developed previously to describe hydrogen bond breaking and reformation dynamics in MeOD.[6] The equation used to fit the pump–probe spectra is

$$
\begin{aligned}
S(t,\omega) = {} & B_1(\omega)e^{-k_R t} + \left(\frac{B_2(\omega)F_{ff}k_R k_{bf}}{(k_{bf}-k_f)(k_f-k_R)(k_{bf}-k_R)}\right)\{(k_{bf}-k_f)e^{-k_R t}+(k_f-k_R)e^{-k_{bf}t}+(k_{bf}-k_R)e^{-k_f t}\} \\
& + \left(\frac{B_2(\omega)F_{fs}k_R k_{bf}}{(k_{bf}-k_s)(k_s-k_R)(k_{bf}-k_R)}\right)\{(k_{bf}-k_s)e^{-k_R t}+(k_s-k_R)e^{-k_{bf}T}+(k_{bf}-k_R)e^{-k_s t}\} \\
& + \left(\frac{B_2(\omega)F_{sf}k_R k_{bs}}{(k_{bs}-k_f)(k_f-k_R)(k_{bs}-k_R)}\right)\{(k_{bs}-k_f)e^{-k_R t}+(k_f-k_R)e^{-k_{bs}t}+(k_{bs}-k_R)e^{-k_f t}\} \\
& + \left(\frac{B_2(\omega)F_{ss}k_R k_{bs}}{(k_{bs}-k_s)(k_s-k_R)(k_{bs}-k_R)}\right)\{(k_{bs}-k_s)e^{-k_R t}+(k_s-k_R)e^{-k_{bs}t}+(k_{bs}-k_R)e^{-k_s t}\}, \qquad (2)
\end{aligned}
$$

where k_R is the rate of excited state decay. The kinetic model[6] contains two rate constants for hydrogen bond breaking, a component for those that break fast, k_{bf}, and a component for those that break slow, k_{bs}. Hydrogen bond reformation was found to occur with two rates as well,[6] some that recombine quickly with rate k_f, and some that recombine slowly with rate k_s. The relative yields of the populations that break and reform hydrogen bonds quickly is F_{ff}; those that break quickly and reform slowly is F_{fs}; those that break slowly and reform quickly is F_{sf}; and those that break and reform slowly is F_{ss}. The fit to each spectrum is a linear combination of the two basis function spectra, which are weighted according to the time dependence determined from the kinetic model. The first basis function $B_1(\omega)$ describes the frequency and time dependence of the excited state and decays with the excited state lifetime, as indicated by the first term in Eq. (2). The second basis function $B_2(\omega)$ grows in with two rates corresponding to hydrogen bond breaking and then decays with two rates corresponding to hydrogen bond reformation. These dynamics are represented by the last four terms in Eq. (2).

Comparison of Figs. 2(a) and 2(b) demonstrates the quantitative agreement between the fit and the pump–probe spectra. At the earliest t delays, the global fit describes the excited state lifetime decay of $k_R = (1/0.8\ \text{ps})$, as seen in the decay of the negative going 1–2 excited state absorption. The gradual collapse and redshift of the positive going features in the first few ps is accurately reproduced by the global fit, even though only two spectra are used as basis functions. The growth of the preserved δ and photoproduct γ spectra, which reach maxima in ~ 4 ps, is reproduced as well. This behavior has been observed previously to result from two time scales of hydrogen bond breaking.[6] Finally, the decay of the preserved δ and photoproduct γ spectra at long t due to hydrogen bond reformation on two time scales is reproduced. The noise that appears in the simulation [see Fig. 2(b)] arises because experimental pump–probe spectra were used to describe the frequency dependence in the simulation. The pump–probe spectra are displayed in Fig. 4. From the fit, we obtain the rate constants for the two rates of hydrogen bond breaking, $k_{bf} = (1/200\ \text{fs})$ and $k_{bs} = (1/2.5\ \text{ps})$. The two rate constants for hydrogen bond reformation obtained from the fit were $k_f = (1/7\ \text{ps})$ and $k_s = (1/20\ \text{ps})$. The relative yields of hydrogen bonds that break and reform quickly, break quickly and reform slowly, break slowly and reform quickly, and break slowly and reform slowly are 5, 2.5, 1, and 7, respectively. These results are in *quantitative agreement with results obtained previously* for MeOD using one-dimensional pump–probe spectroscopy.[6] The earlier experiments did not monitor the appearance and disappearance of the photoproduct γ band. Deuteration of the methyl group would be expected to have little impact on the dynamics other than the change in the vibrational lifetime (discussed above).

Our model's ability to quantitatively fit the pump–probe data using only one basis function to describe the preserved δ and photoproduct γ spectra at all times, t, is the most significant result of the global fitting procedure. Comparison of the two basis functions used to fit the data (see Fig. 4) indicates the spectrum of the preserved δ band is shifted to the red compared with the initially excited δ band. Understanding the origin of this shift provides insight into the mechanism of hydrogen bond evolution and the coupling between the vibrational modes involved in the hydrogen bonded network.

We have been discussing the results in terms of hydrogen bond breaking on the red side of the δ MeOD line (the strongest hydrogen bonds) and the formation of the γ photoproduct, which at first glance appears counterintuitive. Actually, several possible models describing the hydrogen bond population dynamics can explain the observed spectral features in the pump–probe spectra. In the following discussion, we use the results of vibrational echo correlation spectroscopy to unambiguously demonstrate that δ MeOD's on the red side of the δ band selectively break hydrogen bonds, which generates photoproduct γ absorbers that are shifted to higher frequency (Model 4, the red-breaking model described below). We also demonstrate that these conclusions

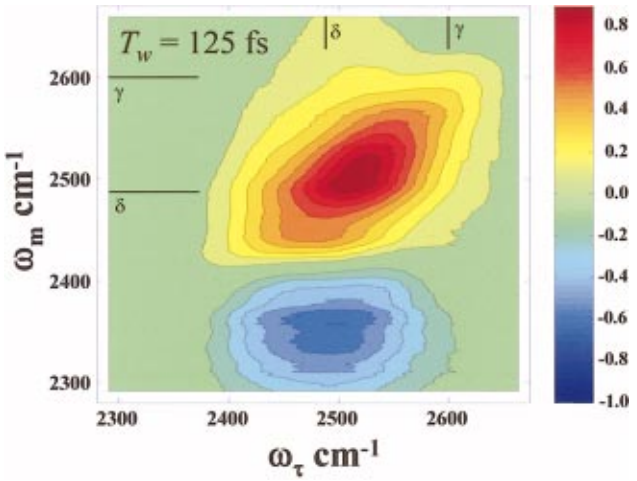

FIG. 5. (Color) The simulated vibrational echo correlation spectrum for $T_w = 125$ fs. The positive going band arises from the 0–1 transition. The negative going band arises from the 1–2 transition. The red edge of the positive going band has contributions from a Fermi resonance with the overtone of the methyl rocking mode.

cannot be drawn from the broad-band IR pump–probe results presented above.

B. Correlation spectra

In correlation spectroscopy, the population and vibrational dephasing dynamics are measured in two frequency dimensions, ω_m and ω_τ. The positions and signs of peaks in the correlation spectra display the history of the various species involved in the hydrogen bonding dynamics. The correlation spectra contain information that cannot be extracted from the pump–probe spectra or from linear absorption spectroscopy. With the additional information contained because of the ω_τ axis and detailed calculations, we are able to unambiguously determine that the red side of the δ band preferentially breaks hydrogen bonds.

Figure 5 is a contour plot of the 2D correlation spectrum of 10 mol% MeOD in CCl_4 with $T_w = 125$ fs. For $T_w > 75$ fs, nonresonant contributions to the signal are negligible. The data have been normalized to the maximum positive signal. The contours represent equal 10% graduations. Correlation spectra were obtained for both MeOD and *d*-MeOD. Other than the differences in the vibrational lifetimes, the correlation spectra of the two species display the identical time dependent features and trends. The data for MeOD will be presented because more extensive data were taken. The positive going band on the diagonal corresponds to the 0–1 transition of the δ band with a contribution from the 0–1 γ band on the blue end. The red end of the positive going 0–1 band is wider and has a different shape than the rest of the band because of contributions from the Fermi resonance (see Fig. 1).[4] The center frequencies of the δ and γ 0–1 transitions are indicated by horizontal and vertical lines in Figs. 5 and 6. The negative going off-diagonal band arises from the 1–2 transition of the δ band. The 1–2 band is off diagonal because it is described by a three level rephasing diagram. The first interaction with the field produces a 0–1 coherence that dephases at the 0–1 transition frequency. The second interaction yields a population in the $\nu = 1$ level, while the third interaction produces a 1–2 coherence that rephases and emits the vibrational echo pulse at the 1–2

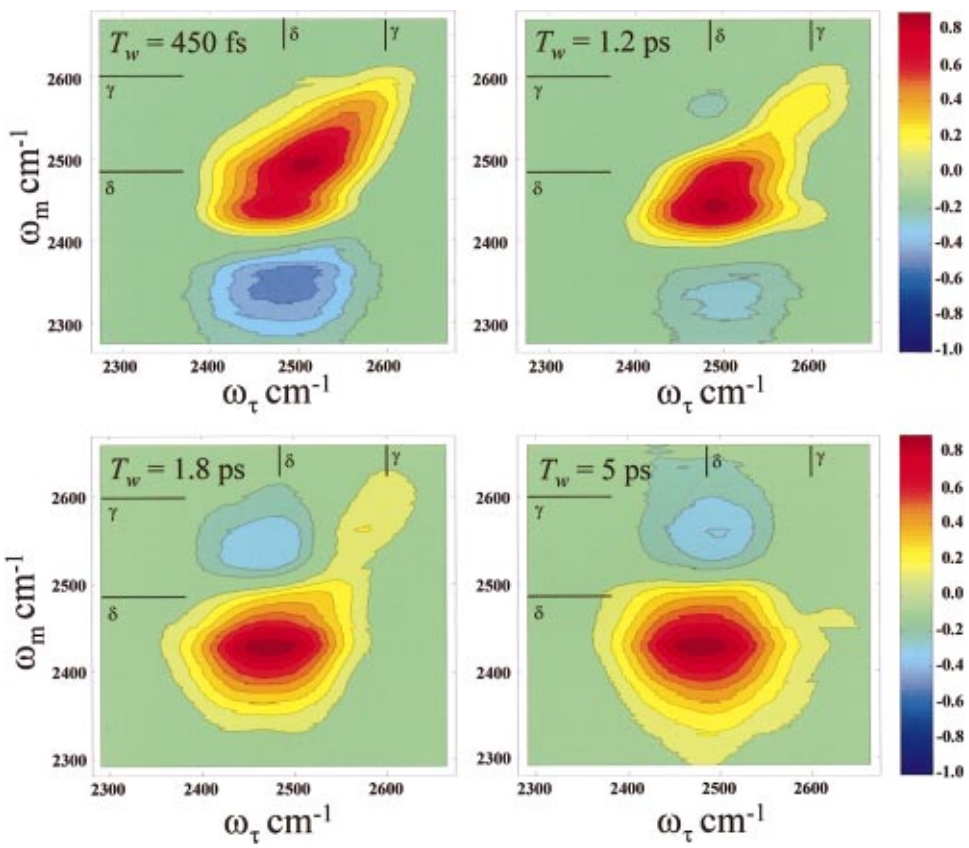

FIG. 6. (Color) Contour plots of the correlation spectra for $T_w = 450$ fs, 1.2 ps, 1.8 ps, and 5 ps. As T_w increases, the off-diagonal negative going 1–2 band (bottom) decays, the main band on the diagonal changes shape by collapsing to the red and shifts somewhat off the diagonal, and a new off-diagonal negative going peak appears (top).

transition frequency, which is shifted to the red by the anharmonicity ($\sim 100\ \mathrm{cm}^{-1}$).[47] It should be noted that the shape of the δ 1–2 transition is distorted on the red edge because the laser spectrum falls off rapidly at lower frequency. Consequently, it does not appear elongated along the diagonal like the 0–1 transition. The γ 1–2 transition is not resolved in the correlation spectrum because it is obscured by the much larger δ 0–1 peak. Similar to the δ 1–2 peak, the pathway leading to the γ 1–2 peak dephases on the γ 0–1 transition and rephases on the γ 1–2 transition, making the peak off-diagonal. The negative going γ 1–2 peak lies in the middle of the positive going δ 0–1 peak along the ω_m axis because of its $\sim 100\ \mathrm{cm}^{-1}$ anharmonicity.[47] As discussed above, the amplitude of the γ transitions are ~ 20 times smaller than the corresponding δ transitions. Although the γ 1–2 peak is not resolved, the correlation spectrum indicates its presence by the asymmetry of the δ 0–1 peak around the diagonal. The presence of the negative going γ 1–2 peak narrows the width of the positive going δ 0–1 peak on its lower right side. The upper left side is not narrowed by overlap with the γ 1–2 peak and so appears broader.

Figure 6, along with Fig. 5, shows five contour plots at $T_w = 125$ fs, 450 fs, 1.2 ps, 1.8 ps, and 5.0 ps for MeOD. The data have been normalized to the maximum positive signal. The contours represent equal 10% graduations. At 125 fs (Fig. 5), the spectrum is dominated by the 0–1 band (positive) and the 1–2 band (negative). In the 450 fs plot, the negative going 1–2 band is less intense, and the 0–1 band is beginning to change shape. The vibrational lifetime of the OD stretch is ~ 0.5 ps, although there is some wavelength dependence to the lifetime.[6] By $T_w = 450$ fs, a good fraction of the initially produced excited state population has decayed to the ground state. Therefore, by the time of the third pulse, the contribution to the signal from the pathway (diagram) that gives rise to the 1–2 band is reduced. By $T_w = 1.2$ ps, the correlation spectrum has changed dramatically. The 1–2 off-diagonal peak is almost gone, and the diagonal δ band has clearly changed shape, contracting to the red along the ω_m axis. A small peak on the blue end of the diagonal 0–1 band has also been uncovered. As the δ band contracts to the red, the remnants of the γ band are uncovered because the γ band has a longer lifetime of ~ 1 ps. The γ 1–2 peak is still not visible even though its 0–1 transition has been uncovered because, as we will demonstrate, only the blue side of the δ 0–1 peak decays completely with the lifetime. The red side is preserved through hydrogen bond breaking. Consequently, the preserved positive going δ 0–1 peak continues to obscure the negative γ 1–2 peak. A new off-diagonal negative going peak appears located above the δ band. In the 1.8 ps plot, the 1–2 peak is gone and the positive going diagonal γ peak is almost gone. The diagonal δ band has contracted further to the red, and it has moved somewhat off of the diagonal. The shift of the position off of the diagonal is progressive; as T_w increases, the δ band contracts and shifts off of the diagonal. By 1.8 ps, the contraction is quite pronounced. The new off-diagonal negative peak located above the δ band has grown considerably in magnitude. For $T_w = 5$ ps, the diagonal γ band is gone. The only remaining features are the δ band that is contracted to the red and the off-diagonal negative going peak. The observed collapse of the band to the red is not influenced by the presence of the Fermi resonance. The identical behavior was observed in *d*-MeOD, which does not have the Fermi resonance.

The T_w dependence of the correlation spectra raises a number of questions: First, why is there a signal for times long compared to the vibrational lifetime? Although we observed the same behavior in the pump–probe spectra, we did not discuss the origin. The peaks in the correlation spectra correspond to different radiation-system quantum pathways that can be represented diagrammatically.[49] After the second interaction with the field (after the second pulse) two pathways contribute to the δ and γ 0–1 peaks. One pathway proceeds through the excited state while another pathway proceeds through the ground state during the population period. In a pump–probe experiment, these pathways correspond to stimulated emission and ground state bleach seen by the probe, respectively. The decay of the excited state pathway into the ground state pathway causes the signal to decay with the excited state lifetime. However, detailed experimental studies[5,6] demonstrate that following vibrational relaxation, $\sim 20\%$ of the initially excited δ's break hydrogen bonds on a very short time scale (~ 200 fs). Breaking a hydrogen bond attached to a δ removes it as a δ absorber. The broken bond eliminates two δ's and creates a γ and a β. Thus, the ground state is not completely filled following complete relaxation of the excited state. This leaves some amplitude in the ground state pathway, although the excited state pathway has decayed completely.

A new quantum pathway is generated when a hydrogen bond breaks. When a δ excited state relaxes and breaks a hydrogen bond, the photoproduct γ is in the ground state of the hydroxyl stretch. The third interaction with the field turns both the preserved δ ground state and the newly formed γ photoproduct into 0–1 coherences. The signals are emitted at the preserved δ 0–1 and at the photoproduct γ 0–1 transition frequencies. Because the preserved δ ground state and the photoproduct γ are spectrally distinct, they can be detected independently, as demonstrated in Figs. 5 and 6. These ground state signals remain for the hydrogen bond recombination time, which is tens of ps.[5,6]

C. Hydrogen bond breaking mechanism

The second question raised by the T_w dependence of the correlation spectra is, why does the δ band shift to the red as T_w becomes longer than the vibrational lifetime? Understanding the origin of this shift provides insight into the mechanism of hydrogen bond evolution and the coupling between the vibrational modes involved in the hydrogen bonded network. To address this question, we have performed detailed calculations to model the correlation spectra, thereby allowing us to quantitatively test four models of hydrogen bond population dynamics. The detailed calculations demonstrate that three of the four models can reproduce the pump–probe spectra presented above, and so cannot be distinguished on that basis. However, the detailed calculations demonstrate the models can be unambiguously distinguished using vibrational echo correlation spectroscopy. The four models are described briefly below:

Model 1: Both δ and γ species *break* hydrogen bonds.

Model 2: Both δ and γ species hydrogen bonds *weaken*.

Model 3: Only δs hydrogen bonds *weaken*.

Model 4: Hydrogen bonds *break* selectively only on the low frequency side of the δ band.

We discussed the pump–probe results in terms of a model in which δ MeODs on the red side of the line selectively break hydrogen bonds and form the γ photoproduct. Hydrogen bond weakening would occur by deposition of vibrational energy (heat) into an oligomer, which would make a hydrogen bond longer on average, that is, weaken it. Models 1–3 assume the δ and γ bleach features are described by their equilibrium frequencies and widths, as measured by FTIR spectroscopy of the sample (see Fig. 1). Thus, these models assume no frequency dependence to the hydrogen bond breaking or weakening that follows vibrational energy relaxation. Model 1 assumes the product γ is also defined by its corresponding equilibrium frequency and width (from the FTIR spectrum). Models 2 and 3 allow the product to have an arbitrary frequency shift (hydrogen bond weakening). Model 4 assumes only a portion of the δ band is preserved through hydrogen bond breaking. Hence, the preserved bleach and product peaks have different spectra than the δ or γ bands observed in the FTIR spectrum. Model 4 is the red-breaking model. We quantitatively compare the four models to the correlation spectra by modeling them as the sum of overlapping two-dimensional Gaussian peak shapes. For a detailed explanation of the fitting procedure, see Appendix A.

The first step is to simulate the $T_w = 125$ fs correlation spectrum, the spectrum prior to hydrogen bond breaking. To simulate the $T_w = 125$ fs correlation spectrum, we included seven peaks as follows: the 0–1 and 1–2 transitions of the δ band, the 0–1 and 1–2 transitions of the γ band, the Fermi resonance peak and the two cross peaks between the Fermi resonance and the δ band. In the subsequent calculations of the $T_w = 5.0$ ps correlation spectrum, the 1–2 transitions of the δ and γ bands do not occur in the fit because excited state relaxation completely depletes the excited states of both species by this T_w delay. The fitting procedure employs two complimentary experiments to further constrain the fit, the linear absorption spectrum (see Fig. 1) and the IR pump–probe spectra (see Figs. 2 and 4).

Many of the parameters used to describe the two-dimensional peaks in the $T_w = 5.0$ ps correlation spectrum are set by fitting the $T_w = 125$ fs correlation spectrum. Therefore, we display the best fit to the $T_w = 125$ fs correlation spectrum in Fig. 7. The experimental data collected at $T_w = 125$ fs are displayed in panel (a) for comparison with the calculated correlation spectrum displayed in panel (b). The data and fit have been normalized to the maximum positive signal. The contours display equal 10% graduations. In this calculation, all the linewidths and positions were fixed to their values obtained from fitting the linear spectrum. The R^2 value of 0.18 [see Eq. (A1.3)] indicates a very accurate fit to the experimental data. Panel (c) displays the projection of the best fit onto the ω_m axis calculated by integrating over the ω_τ axis [see Eq. (A1.4)] compared with the experimental data projected onto the same axis (equivalent of the pump–probe spectrum at $T_w = 125$ fs). Note that the ω_m axis is the vertical axis in the one-dimensional frequency plot. Clearly, the fully constrained best fit is an accurate description of the $T_w = 125$ fs correlation spectrum and pump–probe experimental data.

The correlation spectrum calculated from Model 1 is displayed in Fig. 8. The $T_w = 5.0$ ps experimental data is displayed in panel (a) for comparison with the calculated correlation spectrum displayed in panel (b). For simplicity, we have assumed the spectral diffusion dynamics are complete, causing the peaks to have equal diagonal and antidiagonal widths. In fact, the spectral diffusion is virtually complete as determined by measurements at longer T_w's. The assumption does not change the quality of the fit. The predicted pump–probe spectrum calculated from Model 1 using Eq. (A1.4) is displayed in panel (c). The correlation spectra calculated from Models 2–4 are displayed in Fig. 9, panels (a), (b), and (e), respectively. The $T_w = 5.0$ ps experimental correlation spectrum is displayed for comparison in panel (d). The data and fits displayed in Figs. 8 and 9 have been normalized to the peak of the positive signal. The contours display equal 10% graduations. The right-hand column of one-dimensional frequency plots displays the projection of the experimental data compared with the projections calculated from Model 3 [panel (c)] and from Model 4 [panel (f)]. Note that the ω_m axis is the vertical axis in the one-dimensional frequency plots displayed in Figs. 8 and 9. The horizontal axis displays the peak intensity integrated over the ω_τ axis. The R^2 values displayed in the lower left corner of the two-dimensional spectra are calculated using Eq. (A1.3). These numbers evaluate the accuracy with which each calculated correlation spectrum reproduces the $T_w = 5.0$ ps data.

We now discuss the results of using the modeling procedure described above and in Appendix A to determine which of the four models best describes the experimental data. For a detailed discussion of the parameters used for each model, see Appendix B. We first consider Model 1, both δ and γ species *break* hydrogen bonds (see Fig. 8). When a δ breaks a hydrogen bond, a γ and a β are produced, and when a γ breaks a hydrogen bond, an α is produced. The model is similar to the early hydrogen bond predissociation mechanism.[14–17,50] The central premise of this model suggests the very intuitive idea that the $T_w = 5.0$ ps experimental correlation spectrum can be reproduced by an appropriate summation of two-dimensional Gaussian peaks whose shapes are described by the equilibrium δ and γ bands, as

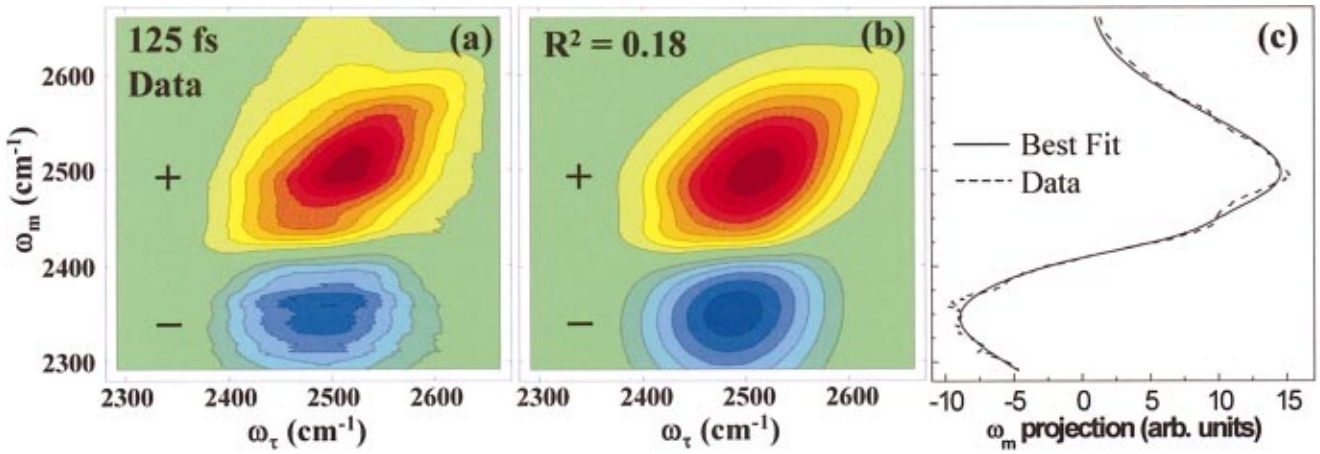

FIG. 7. (Color) Comparison of the $T_w = 125$ fs experimental correlation spectrum [panel (a)] with the calculated correlation spectrum using the two-dimensional Gaussian model [panel (b)]. The contours display equal 10% graduations of the normalized data. Panel (c) displays the comparison of the projection onto the ω_m axis of the calculated spectrum to the experimental data. Note that the ω_m frequency axis is the vertical axis in the one-dimensional plot. The horizontal axis displays the peak amplitude integrated over the ω_τ axis. The fit accurately reproduces the data. Many of the parameters used to fit the $T_w = 5.0$ ps correlation spectrum are obtained from this fit. See text for details.

determined from the linear absorption spectrum. Note that the equilibrium δ and γ bands described well the $T_w = 125$ fs experimental correlation spectrum (see Fig. 7). By inspection, it is obvious that this assumption results in a poor representation of the experimental data. For comparison, we indicate the R^2 value of the calculated correlation spectrum [R^2 for Model 1 = 49, see Eq. (A1.3)], which contrasts with the typical best-fit values of <0.2. The discrepancies are not only obvious in the correlation spectrum, but also in the calculated pump–probe spectrum compared with the data [see Fig. 8, panel (c)]. Model 1 predicts the γ product, which forms when a δ breaks a hydrogen bond, should appear at ($\omega_m = 2600\ \mathrm{cm}^{-1}$, $\omega_\tau = 2490\ \mathrm{cm}^{-1}$). The negative going product signal above the δ band in the $T_w = 5.0$ ps correlation spectrum appears at ($\omega_m \sim 2560\ \mathrm{cm}^{-1}$, $2490\ \mathrm{cm}^{-1}$). This peak is redshifted a full half-width of the equilibrium γ peak away from its equilibrium frequency along the ω_m axis. In addition, the central frequency of the preserved δ bleach peak is substantially shifted away from the experimentally observed frequency. Even the pump–probe spectrum can show that Model 1 is not correct. Though this model is very intuitive, it cannot adequately describe the data.

Next, we consider Models 2 and 3. Refer to Appendix B for a detailed assignment of band positions and widths in these models. These models are very similar, with the exception that in Model 2, both δ's and γ's weaken hydrogen bonds, while in Model 3 only δ's weaken hydrogen bonds. Although there is no physical basis for Model 3, we consider it because it produces a correlation spectrum which qualitatively looks like the data. When a band undergoes weakening, the entire band is weakened. In other words, δ and/or γ MeOD's weaken hydrogen bonds uniformly across their respective bands. Consequently, the preserved ground state bleaches appear with their equilibrium positions and widths (determined from the linear spectrum). There is no frequency dependence to the probability of weakening a hydrogen

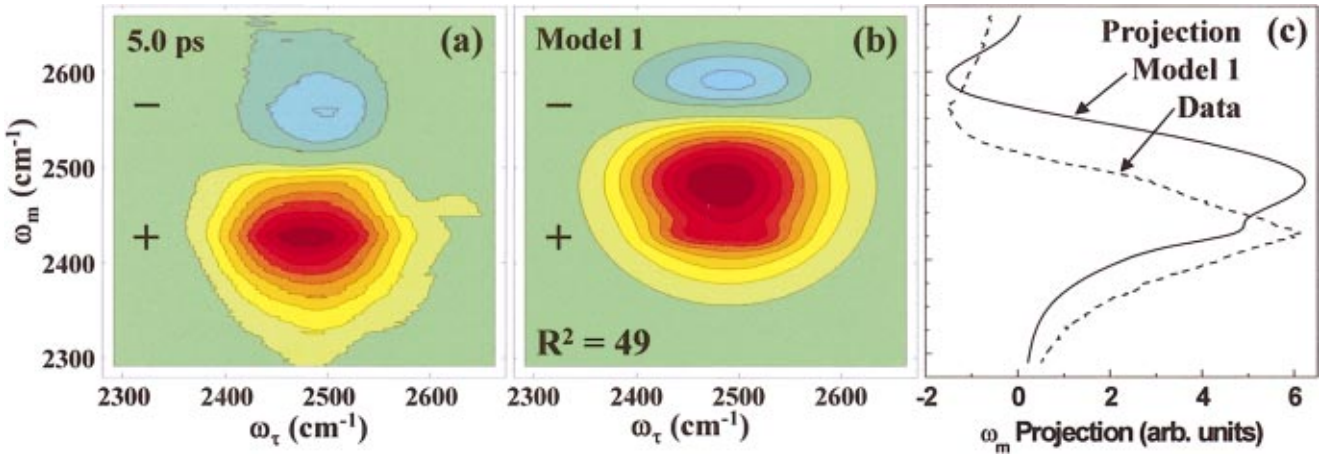

FIG. 8. (Color) Contour plots of the experimental $T_w = 5.0$ ps correlation spectrum, panel (a), compared with the calculated correlation spectrum from Model 1, panel (b). The contours display equal 10% graduations of the normalized data. The projection of the calculated correlation spectrum compared to the data is displayed in panel (c). Note that the ω_m frequency axis is the vertical axis in panel (c). The horizontal axis displays the peak amplitude integrated over the ω_τ axis. Model 1 does not accurately describe the experimental data.

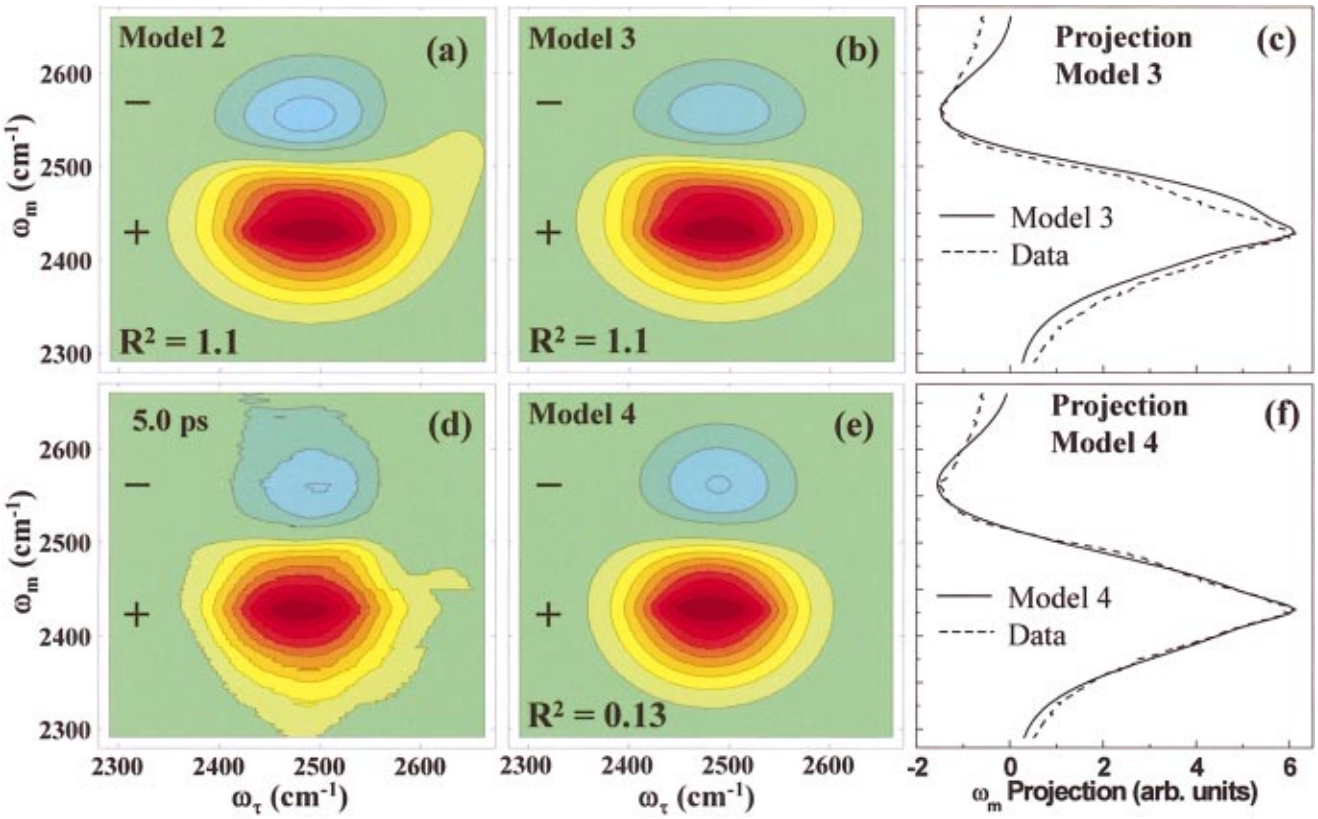

FIG. 9. (Color) Contour plots of calculated correlation spectra from Models 2–4 displayed in panels (a), (b), and (e), respectively. The $T_w = 5.0$ ps experimental correlation spectrum is displayed in panel (d) for comparison. The contours display equal 10% graduations of the normalized data. The projections of the Models 3 and 4 are compared to the experimental data in the one-dimensional frequency plots, panels (c) and (f), respectively. Note that the ω_m frequency axis is the vertical axis in the one-dimensional plot. The horizontal axis displays the peak amplitude integrated over the ω_τ axis. Model 4, the red-breaking hydrogen bond model, provides a much more accurate fit to the data than either Models 2 or 3, the hydrogen bond weakening models. In addition, the fitting parameters from Model 4 are physically meaningful, unlike Models 2 or 3. See text for details.

bond. Weakening a hydrogen bond moves the hydroxyl stretch to higher frequency (to the blue). Therefore, the ''photoproducts'' are moved to the blue. In this respect, Models 2 and 3 are the same as Model 1. The difference between these models comes in the frequency shift of the photoproduct. By assuming that hydrogen bonds weaken rather than break, we allow arbitrary adjustment of the position of the product peak along the ω_m axis. The product peak is taken to have identical width characteristics as the weakened ground state. The shift due to weakening of the hydrogen bonds, Δ_w, is defined as the splitting between the preserved δ bleach, $\omega_{m,\delta}$, and the product peak, $\omega_{m,p}$,

$$\Delta_w = \omega_{m,p} - \omega_{m,\delta}. \tag{3}$$

The magnitude of Δ_w describes the perturbation of the hydroxyl stretch frequency that results from weakening the hydrogen bonds associated with it.

Measurements of spectral diffusion show that it is almost, but not quite complete by $T_w = 5.0$ ps. For simplicity, we take the spectral diffusion to be complete. If we assume the opposite limit of virtually no spectral diffusion, the best fit to the correlation spectrum is poor. (The R^2 values [see Eq. (A1.3)] for little spectral diffusion of Models 2 and 3 are ~ 14 and ~ 8, respectively. Typical best fit values of R^2 are < 0.2.)

With full spectral diffusion, qualitatively good agreement between calculations based on Models 2 and 3 and the experimental correlation spectra is obtained [Fig. 9, panels (a) and (b)]. Model 2 predicts that a positive shoulder appears at the upper right of the preserved δ bleach peak because the γ bleach is preserved by hydrogen bond weakening, $R^2 = 1.1$. This shoulder does not appear in the data. Model 3 does not predict this shoulder because only the δ band has weakened hydrogen bonds, $R^2 = 1.1$. The pump–probe spectra corresponding to Models 2 and 3 are indistinguishable as well (the pump–probe spectrum of Model 2 is not shown). Although Models 2 and 3 cannot be discriminated either by their R^2 values or by their pump–probe spectra, they can be distinguished by their two-dimensional correlation spectra peak shapes. Therefore, Model 3 describes the experimental data more accurately than Model 2.

In addition to the shapes of the correlation spectra, there are amplitudes. The ratio of the amplitude of the $T_w = 125$ fs experimental correlation spectrum to the $T_w = 5$ ps experimental correlation spectrum is well defined. The calculated correlation spectra should have approximately the same amplitude in addition to the same shape as the experimental data. Although the correlation spectrum calculated from Model 3 does a reasonable job of describing the shape of the experimental data [compare panels (b) and (d)], the

TABLE I. Summary of fitting parameters from calculation of correlation spectra.

Model (No.)	$\omega_{m,\delta}$ (cm^{-1})	$\omega_{\tau,\delta}$ (cm^{-1})	Δ_w (cm^{-1})	FWHM$_\delta$ (cm^{-1})	A_δ[b]	A_p	R^2
Red break (4)	2430[a]	2480[a]	130[a]	130[a]	0.32[a]	0.2[a]	0.13
Weaken (2–3)	2490	2490	5[a]	150	>4[a]	>4[a]	$\geqslant 1.1$
Break (1)	2490	2490	100	150	0.32[a]	0.3[a]	49

[a]Fitting parameter.
[b]Amplitude relative to fit of 125 fs correlation spectrum.

parameters required to force the model to reproduce the necessary amplitude are not physically meaningful. The fitting parameters are summarized in Table I. Every fitting parameter not listed in Table I was fixed from the fit of the $T_w = 125$ fs correlation spectrum. In order to force the ground state bleach and product peaks to appear near the frequencies observed in the experimental data, a shift due to hydrogen bond weakening, Δ_w, of only 5 cm^{-1} is required. The peaks overlap severely because they are so wide (FWHM $= 150$ cm^{-1} along both ω_m and ω_τ, a characteristic enforced by the linear spectrum). Therefore, they almost completely cancel. Consequently, *Model 3 requires the amplitude of the preserved δ band peak, A_δ, at $T_w = 5.0$ ps to be 4.4 times larger than its initial value at $T_w = 125$ fs, which implies that the preserved bleach must be 8.8 times larger than its initial value. The amplitude of the product peak, A_p, is also >4 times larger than the initial amplitude of the δ band.* Only the preserved bleach contributes to the 0–1 signal at $T_w = 5.0$ ps because vibrational relaxation depletes the excited state. If every methanol that was excited broke a hydrogen bond, the 0–1 peak would be no more than half its initial magnitude. If we force the amplitude of the 0–1 and product peaks to be more reasonable, say half their initial magnitude, the product peak must be shifted ~ 100 cm^{-1} to have the proper amplitude of the calculated correlation spectrum. This shift is so large that the calculated correlation spectrum looks the same as that predicted by Model 1 (see Fig. 8), which does not describe the data. We conclude that Model 3 cannot describe the hydrogen bond population dynamics displayed in the correlation spectra. It should be noted that Model 2 predicts even less reasonable fitting parameters. According to Model 2, the amplitude of the preserved bleach is 10.2 times the original bleach.

Finally, we consider Model 4, hydrogen bonds *break* selectively only on the low frequency side of the δ band. See Appendix B for a detailed description of the fit. Model 4 differs from Models 1–3 in that we relax the constraint that the preserved δ bleach must be described by the equilibrium width and position of the δ band. Lifting this constraint is tantamount to allowing a portion of the δ band to selectively break hydrogen bonds, which is the essence of the red-breaking model. The correlation spectrum calculated from Model 4 is displayed in panel (e) of Fig. 9. The R^2 value, calculated from Eq. (A1.3), is ~ 8 times smaller than the R^2 value calculated from either Models 2 or 3, indicating that Model 4 is a much more precise description of the $T_w = 5.0$ ps experimental correlation spectrum. The projection of the calculated correlation spectrum from Model 4, displayed in panel (f), agrees much more closely with the data than do Models 1–3. The ability of Model 4 to describe the experimental data much more accurately than Models 1–3 results from the fact that we allowed the position of the preserved δ bleach to move in the (ω_m, ω_τ) plane in the fit. The important point is that the preserved δ bleach *cannot* be described by the equilibrium δ band. The data indicates only the low frequency side of the δ band is preserved through hydrogen bond breaking.

Model 4 also comes close to the correct amplitude for the $T_w = 5$ ps correlation spectrum in contrast to Models 2 and 3. The Model 4 calculations give a preserved δ bleach of $\sim 60\%$ of the initial $T_w = 125$ fs bleach, which indicates $\sim 60\%$ of the methanol molecules that were excited broke a hydrogen bond. Independent experiments studying hydrogen bond population dynamics in MeOD oligomers found that 20% of the hydrogen bonds are broken in ~ 200 fs and then another $\sim 20\%$ break on a slower time scale of ~ 2 ps.[5,6] Extension of these experiments to this model predicts the preserved bleach at $T_w = 5.0$ ps should be $\sim 40\%$ of the initial bleach ($\sim 20\%$ of the initial 0–1 signal). The magnitude of preserved bleach predicted by Model 4 is in reasonable agreement with these experiments. If the fact that spectral diffusion is not strictly complete at $T_w = 5$ ps were taken into account in the model, the agreement would probably be significantly better. Nonetheless, Model 4 produces the correct correlation spectrum amplitude for physically reasonable parameters and a much better description of the shapes and peak positions than the other models.

Model 4 yields a frequency shift of the product peak of ~ 130 cm^{-1}. This shift demonstrates that we observe selective hydrogen bond *breaking* on the red side of the band rather than selective hydrogen bond weakening. When a monomer becomes a hydrogen bond donor, its average frequency redshifts ~ 100 cm^{-1}. When a hydrogen bond donor accepts an additional hydrogen bond, its average frequency redshifts an additional ~ 100 cm^{-1}. By extension, the blueshift of ~ 130 cm^{-1} predicted by Model 4 suggests a strong hydrogen bond has broken.

There is general agreement in the literature that the red side of the hydroxyl stretch of a hydrogen bonding liquid corresponds to stronger hydrogen bonds.[1,11,16,19,39,40,42,44] Very strong evidence for the correlation between the hydroxyl stretch frequency and the hydrogen bond strength in solids is obtained from correlating crystallographic data and spectroscopic data.[51] From the crystallographic data, the length of the hydrogen bond can be determined. A shorter length corresponds to a stronger bond. Observations on a large number of compounds show that as the bond shortens, the hydroxyl stretch frequency shifts to the red. The fact that the crystallographic/spectroscopic relationship also applies to liquids follows from three observations about the hydroxyl

stretch of hydrogen bonded liquids, such as water and alcohols. First, molecules that form stronger hydrogen bonds display larger redshifts in their hydroxyl stretch than molecules that form weak hydrogen bonds.[1,39,40] Second, the hydroxyl stretch band is inhomogeneously broadened.[3,4,8,11,19,20,22,42] In a hydrogen bonding liquid, the lengths and strengths of hydrogen bonds vary substantially, giving rise to the broad inhomogeneously broadened hydroxyl stretch band. Finally, the hydroxyl stretch frequency of water (the prototypical hydrogen bonded liquid) varies continuously from its low temperature, icelike spectrum (large redshift, strong hydrogen bonds) to its high temperature vaporlike spectrum (small redshift, weak hydrogen bonds) when the temperature is varied from the freezing to boiling points.[44] Falk and Ford concluded that hydrogen bonds varied continuously in strength rather than having a fixed strength.

In terms of the correlation between the hydrogen bond strength and hydroxyl stretch frequency, we consider the $\sim 130\ \mathrm{cm}^{-1}$ shift. If the frequency shift from forming an average strength hydrogen bond is $\sim 100\ \mathrm{cm}^{-1}$, then the frequency shift from breaking a strong hydrogen bond might be expected to be $>100\ \mathrm{cm}^{-1}$. The frequency shift of the product peak is fully consistent with preferentially breaking the strongest hydrogen bonds in the δ band following vibrational energy relaxation of the hydroxyl stretch.

In the above analysis, we assumed the spectral diffusion dynamics are complete, which simplified the models. While much of the spectral diffusion has occurred by 5 ps, the dynamics are not yet complete. The assumption of complete spectral diffusion at 5 ps does not change the analysis presented here. As we will report in a forthcoming publication,[52] we find a significant slow component to the dynamics that extends into the tens of ps time scale, which we assign to thermal equilibration within the oligomers.[52] As thermal equilibration occurs, memory of the hydrogen bond strengths is erased and the oligomers reach their thermal distribution. However, on shorter time scales, the memory of the hydrogen bond strengths has not been erased, which permits us to observe breaking of the strongest hydrogen bonds.

Breaking of the strongest hydrogen bonds is at first surprising. Hydrogen bond breaking follows vibrational energy relaxation (VER). The details of which low frequency modes will be involved in VER depend on the initial excitation energy and the modes that are available to receive the energy.[53] VER into intramolecular modes dominates the hydroxyl stretch relaxation pathway in methanol and water.[23,27,54] For example, Iwaki and Dlott excited the hydroxyl stretch of methanol and, within their time resolution of ~ 1 ps, observed excitation of every bending mode in the molecule.[54]

Preferential breaking of the strongest hydrogen bonds can occur if vibrational relaxation on the low energy side of the line populates different modes than vibrational relaxation on the high energy side of the line, and the modes populated through the lower energy relaxation pathway are more effective at breaking hydrogen bonds. Significant support for different relaxation pathways comes from the IR pump/Raman probe experiments of Iwaki and Dlott, who observed that the pathway for vibrational relaxation was different on the red and blue sides of the hydroxyl stretching band in OH methanol.[54] Excitation on the red side led to vibrational relaxation that produced substantially more relative population of hydroxyl bends compared to excitation on the blue side that put much more population into the CH bends and other modes.[54] The hydroxyl bends would be expected to be strongly coupled to the hydrogen bond in contrast to CH bends.

Further support for different relaxation pathways for the red and blue sides of the hydroxyl stretch come from a study of vibrational relaxation of the OH stretch of HOD in liquid D_2O.[55] It has been shown that the modes that are excited following VER depend on the energy of the OH stretch, that is, its position in the inhomogeneously broadened hydroxyl stretch band.[55] The above considerations suggest the following. The pathways for VER depend on the frequency of the hydroxyl stretch, and therefore, the strengths of the hydrogen bonds. On the red side of the line, the pathways are different from those on the blue side of the line. The pathways on the red side of the line lead to population of intramolecular and intermolecular modes that are effective at hydrogen bond breaking, while the blue side pathways populate modes that are not effective.

Using vibrational echo correlation spectroscopy, we have elucidated the complicated hydrogen bond population dynamics in MeOD oligomers with great detail and demonstrated vibrational echo correlation spectroscopy as a new probe of hydrogen bond dynamics. In some, but not all situations, information obtained by vibrational echo correlation spectroscopy can also be obtained using frequency resolved pump–probe experiments.[8] Model 4 was selected over Model 3 because of Model 3's unrealistic prediction of the amplitude of the ground state bleach at long time. In the specific case of these two models, the unrealistic amplitude predicted by Model 3 would also be apparent by fitting the spectrally resolved pump–probe data. However, spectrally resolved pump–probe experiments do not provide the same information as correlation spectroscopy in all situations. For example, Models 2 and 3 could only be distinguished on the basis of their two-dimensional peak shapes. In general, the extra frequency dimension (ω_τ, horizontal axis) greatly enhances sensitivity to intricate population dynamics (such as those observed in MeOD) as well as revealing spectral diffusion dynamics within those populations. Spectral diffusion dynamics can in principle be obtained using transient hole burning (THB) spectroscopy. Indeed, vibrational echo correlation spectroscopy is like THB *without the time bandwidth product limitation*. However, the combined benefits of increased sensitivity afforded by the two-dimensional absorptive peak shapes, the ability to measure the global dynamics at all applicable frequencies, and the ability to avoid the time bandwidth product inherent to THB make vibrational echo correlation spectroscopy a powerful new probe of structure and dynamics.

IV. CONCLUDING REMARKS

The results of vibrational echo correlation spectroscopy with full phase information have been used to examine aspects of the hydrogen bond dynamics of methanol-OD in

CCl_4. By using extremely short pulses (<50 fs), it is possible to excite the entire very broad hydroxyl-stretching band including the 1–2 transition. Vibrational echo correlation spectroscopy combined with detailed calculations make it possible to explicate the population dynamics of hydrogen bond evolution with considerable clarity and detail.

At short time, the correlation spectrum (see Fig. 5) is dominated by the hydrogen bonded OD stretch 0–1 transition (positive going peak) and the 1–2 transition (negative going peak). However, the stimulated vibrational echo signal can be observed for times long compared to the vibrational lifetime (~ 500 fs) because of the breaking of hydrogen bonds. As T_w is increased to the time scale of and beyond the vibrational lifetime, the broad diagonal δ band contracts to the red side of the line and shifts off of the diagonal. As the hydrogen bonds break, the off-diagonal photoproduct γ peak grows in.

Detailed calculations used to model the experimental correlation spectra demonstrate that the hydroxyls with absorption on the red side of the δ band (strong hydrogen bonds) selectively break hydrogen bonds following vibrational energy relaxation. The preserved ground state on the red side of the δ band in the $T_w = 5.0$ ps correlation spectrum can only be described by a model in which the red side of the band selectively breaks hydrogen bonds while the blue side does not. It is proposed that the strong hydrogen bonds (red side of the hydroxyl stretch band) are selectively broken because the low frequency modes that are excited by vibrational energy relaxation of the hydroxyl stretch differ from those that are excited by VER of the higher frequency hydroxyl stretches (weaker hydrogen bonds).

ACKNOWLEDGMENTS

We would like to thank Professor James L. Skinner, Department of Chemistry, University of Wisconsin at Madison, for useful suggestions pertaining to this work. This work was supported by the AFOSR (Grant No. F49620-01-1-0018), the Department of Energy (Grant No. DE-FG03-84ER13251), the National Science Foundation (DMR-0088942), and the National Institutes of Health (1RO1-GM61137).

APPENDIX A: CORRELATION SPECTRUM MODELING PROCEDURE

We quantitatively compare the four models of hydrogen bond breaking to the correlation spectra by modeling them as the sum of overlapping two-dimensional Gaussian peak shapes having the following form:

$$S(\omega_m,\omega_\tau) = S_L(\omega_m)\sum_i [A_i \exp(-(\cos(\theta)(\omega_m-\omega_{m,i}) + \sin(\theta)(\omega_\tau-\omega_{\tau,i}))^2/2\sigma_{d,i}^2) \times \exp(-(\sin(\theta)(\omega_{m,i}-\omega_m) + \cos(\theta)(\omega_\tau-\omega_{\tau,i}))^2/2\sigma_{a,i}^2)]. \quad \text{(A1.1)}$$

The combined spectrum of the first two laser pulses, $S_L(\omega_m)$, influences the correlation spectrum along the ω_m axis. This influence is accounted for by multiplication of the calculated correlation spectrum by the laser spectrum, $S_L(\omega_m)$. The summation is over all two-dimensional peaks that contribute to the correlation spectrum. The parameters A_i describe the amplitudes of the two-dimensional peaks. The terms including the angle θ reflect a 45° coordinate transformation from the (ω_m,ω_τ) plane to the (ω_d,ω_a) plane (the plane constructed from the diagonal and antidiagonal axes). This transformation allows the diagonally elongated peak shapes to be described by a simple two-dimensional Gaussian function. The positions $\omega_{m,i}$ and $\omega_{\tau,i}$ reflect the position of the ith peak in the (ω_m,ω_τ) plane. The widths of the peaks along the diagonal and antidiagonal are represented by $\sigma_{d,i}$ and $\sigma_{a,i}$, respectively. The diagonal and antidiagonal widths for the ith peak are constrained to produce a total linewidth equal to the corresponding linear linewidth, FWHM_i, which we obtain by fitting the FTIR spectrum of the sample (see Fig. 1). The constraint is enforced in the fitting procedure by the following relationship between $\sigma_{d,i}$, $\sigma_{a,i}$, and FWHM_i:

$$\sigma_{a,i} = \{[(\mathrm{FWHM}_i/2.35)^2 - (\sin(\theta))^2\sigma_{d,i}^2]/(\cos(\theta))^2\}^{1/2}. \quad \text{(A1.2)}$$

Consequently, for each peak, only one independently adjustable parameter is used to determine the two-dimensional shape of the peak. The only exception is the 1–2 transition of the δ band in the $T_w = 125$ fs correlation spectrum. This peak shape is distorted by the red edge of the laser spectrum. Consequently, this highly constrained model was not used to fit this peak. The full width at half maximum of the Fermi resonance and its cross peaks with the δ band are determined from a best fit to the $T_w = 125$ fs correlation spectrum (see Fig. 7).

The best fits to the correlation spectra are obtained by minimizing the integral over the square of the residual volume,

$$R^2 = 100\times\frac{\int\int (S_{\mathrm{Corr}}(\omega_m,\omega_\tau) - S_{\mathrm{Fit}}(\omega_m,\omega_\tau))^2 \,\mathrm{abs}\,\, (S_{\mathrm{Corr}}(\omega_m,\omega_\tau))\, d\omega_t\, d\omega_m}{\int\int \mathrm{abs}(S_{\mathrm{Corr}}(\omega_m,\omega_\tau))^3\, d\omega_t\, d\omega_m}, \quad \text{(A1.3)}$$

resulting from subtracting the two-dimensional Gaussian fit, $S_{\mathrm{Fit}}(\omega_m,\omega_\tau)$, from the experimental correlation spectrum, $S_{\mathrm{Corr}}(\omega_m,\omega_\tau)$. The residual volume is weighted by the absolute magnitude amplitude of the correlation spectrum and normalized by the total volume raised to the appropriate power. This evaluation scheme emphasizes the peaks in the correlation spectrum over the wings and the area containing no signal. Much of the area in the two-dimensional frequency map contains no signal. Small amounts of noise in these areas can grow to dominate the sum of the squares of the residuals due to the large area over which they are integrated. This problem is avoided by weighting the residuals according to Eq. (A1.3).

The fitting procedure uses two complementary experiments to constrain the best fit of the two-dimensional correlation spectra, the linear absorption spectrum (see Fig. 1) and the IR pump–probe spectra (see Figs. 2 and 4). The calculated two-dimensional fit is projected onto the ω_m axis by integrating over the ω_τ axis to calculate the pump–probe spectrum, $S_P(\omega_m)$, corresponding to the fit

$$S_P(\omega_m)=\int S_{\mathrm{fit}}(\omega_m,\omega_\tau)d\omega_\tau. \tag{A1.4}$$

The two-dimensional fit is constrained to reproduce the IR pump–probe spectrum when projected onto the ω_m axis. In practice, the fit is compared to the projection of the experimental correlation spectrum. The projection of the experimental correlation spectrum very accurately reproduces its corresponding IR pump–probe spectrum because the pump–probe spectrum is used as input to the phasing process in the analysis of the experimental correlation spectrum. Consequently, comparison of the fits with the projected experimental correlation spectrum is no different than comparing to the pump–probe spectrum. Finally, the two-dimensional Gaussian peak positions and total widths are constrained to match those obtained by fitting the FTIR spectrum of the sample. Inhomogeneity in the hydroxyl stretch causes the two-dimensional Gaussian peaks in the $T_w=125$ fs correlation spectrum to be elongated along the diagonal (see Fig. 5). The widths along the diagonal and antidiagonal are related to the total linewidth according to Eq. (A1.2). This constraint is used to fit the $T_w=125$ fs correlation spectrum as well as every model used to describe the $T_w=5.0$ ps correlation spectrum. The only exception to this constraint is Model 4, the red breaking model, whose implicit proposition is that this constraint is not valid. High quality fits to the correlation spectra have R^2 values of <0.2 [see Eq. (A1.3)]. This value is larger for models 1–3 because they cannot accurately describe the data.

The relative amplitudes of the δ and γ peaks in Models 1 and 2 are determined from the best fit to the $T_w=125$ fs correlation spectrum displayed in Fig. 7. The ratio of the δ:γ amplitudes from the fit is $\sim 7:1$, which is consistent with the ratio of their extinction coefficients.[48] The positions and amplitudes of the Fermi resonance peaks used in all four models are fixed from the fit of the $T_w=125$ fs correlation spectrum.

APPENDIX B: MODELS OF HYDROGEN BOND DYNAMICS

This Appendix summarizes the detailed peak positions and widths used to model the two-dimensional correlation spectra. It is designed to complement the information provided in the main text.

Model 1

Model 1 is similar to the hydrogen bond predissociation mechanism that has been commonly invoked in the literature to explain the hydrogen bond population dynamics.[14–17,50] In this model, we assume all species appear at their equilibrium frequencies and widths along both ω_m and ω_τ axes. Therefore, the δ bleach appears at ($\omega_{m,\delta}=2490\ \mathrm{cm}^{-1}$, $\omega_{\tau,p}=2490\ \mathrm{cm}^{-1}$) and has a $\mathrm{FWHM}_\delta=150\ \mathrm{cm}^{-1}$ along both axes. The γ bleach appears at ($\omega_{m,\gamma}=2600\ \mathrm{cm}^{-1}$, $\omega_{\tau,\gamma}=2600\ \mathrm{cm}^{-1}$) with a $\mathrm{FWHM}_\gamma=80\ \mathrm{cm}^{-1}$ along both axes. The photoproduct γ peak appears at ($\omega_{m,p}=2600\ \mathrm{cm}^{-1}$, $\omega_{\tau,p}=2490\ \mathrm{cm}^{-1}$). We assume different FWHM for the two axes, $\mathrm{FWHM}_{m,p}=80\ \mathrm{cm}^{-1}$ and $\mathrm{FWHM}_{\tau,p}=150\ \mathrm{cm}^{-1}$ because the γ product dephased as a δ (ω_τ axis width) but emitted as a γ (ω_m axis width). The product α species do not appear in the spectral window. Thus all the frequency positions and widths are fixed by the linear spectrum in this model. Only the amplitudes of the preserved bleach and product peaks are adjusted in Model 1 to fit the $T_w=5.0$ ps correlation spectrum and the pump–probe spectrum. These parameters are summarized in Table I.

Models 2 and 3

These models are the hydrogen bond weakening models. We assume when a band undergoes weakening, the *entire* band is weakened. Consequently, the preserved ground state bleaches appear with their equilibrium positions and widths, similar to Model 1. However, the frequency shift of the product peaks is allowed to vary in order to provide the best fit of the data. The position of the product along the ω_τ axis is fixed. The bleach features are assigned the same frequencies and widths as in Model 1. The product of the weakened δ appears at ($\omega_{m,\delta}=2490+\Delta_w\ \mathrm{cm}^{-1}$, $\omega_{\tau,\delta}=2490\ \mathrm{cm}^{-1}$) and the product of the weakened γ appears at ($\omega_{m,\gamma}=2600+\Delta_w\ \mathrm{cm}^{-1}$, $\omega_{\tau,\gamma}=2600\ \mathrm{cm}^{-1}$). [$\Delta_w$ is defined by Eq. (3), see main text.] We describe the widths of the photoproduct distributions by their corresponding parent distributions. So, the weakened δ photoproduct has a total $\mathrm{FWHM}_{\delta,p}$ of $150\ \mathrm{cm}^{-1}$ and the weakened γ photoproduct has a $\mathrm{FWHM}_{\gamma,p}$ of $80\ \mathrm{cm}^{-1}$. The amplitudes of both δ and γ ground state bleaches as well as the Fermi resonance peaks are all scaled by a single fitting parameter. The amplitudes of the corresponding photoproduct peaks are all scaled by another fitting parameter. In total, three parameters, two amplitudes and the shift, Δ_w, are adjusted to fit the $T_w=5.0$ ps correlation spectrum and the corresponding pump–probe spectrum. These parameters are summarized in Table I.

Inhomogeneously broadened transitions appear as peaks elongated along the diagonal in vibrational echo correlation spectroscopy. Consequently, we must consider spectral diffusion when modeling the $T_w=5.0$ ps data. We assumed two limits to describe the influence of spectral diffusion on the

calculated correlation spectra. The first limit assumes that no additional spectral diffusion occurs by $T_w = 5.0$ ps that has not already occurred by $T_w = 125$ fs. In this limit, we use the identical peak shapes for the δ and γ bands that provide the best fit to the $T_w = 125$ fs correlation spectrum (see Fig. 7). The best fits to the $T_w = 5.0$ ps correlation spectrum had R^2 values of 14 and 8, ~ 70 and ~ 40 times larger than the best fit value, respectively. The second limit assumes that spectral diffusion is complete by $T_w = 5.0$ ps. In this limit, all the peaks that contribute to the calculated correlation spectra are round, having the same widths along both ω_m and ω_τ axes. Experiments show that spectral diffusion is almost complete by $T_w = 5.0$ ps. The second spectral diffusion limit provides a much more accurate description of the experimental data at $T_w = 5.0$ ps. The R^2 values for Models 2 and 3 are both 1.1. However, we are able to discriminate between Models 2 and 3 by visual inspection of the correlation spectra. Model 2 assumes both δ and γ bands weaken hydrogen bonds, which results in a preserved bleach (positive signal) at ($\omega_m = 2600\ \mathrm{cm}^{-1}$, $\omega_\tau = 2600\ \mathrm{cm}^{-1}$). Because hydrogen bonds weaken rather than break in this model, the product of the γ band is a weakened γ that appears at ($\omega_m = 2600 + \Delta_w\ \mathrm{cm}^{-1}$, $\omega_\tau = 2600\ \mathrm{cm}^{-1}$). These features result in a positive shoulder on the upper right of the preserved δ band in Fig. 9, panel (a). The experimental data at $T_w = 5.0$ ps do not display the positive shoulder on the upper right of the preserved δ bleach. Model 3 does not predict this shoulder, since in this model only δ's weaken hydrogen bonds. Therefore, Model 3 is a more accurate description of the experimental data. As discussed in the text, neither Models 2 or 3 get the amplitude of the correlation spectrum right. They are factors of 8.8 and 10.2 off, respectively.

Model 4

Model 4 differs from Models 1–3 in that we relax the constraint that the preserved δ bleach must be described by the equilibrium width and position of the δ band. We allow the position of the preserved δ band in the (ω_m, ω_τ) plane and its overall width to vary. Within the complete spectral diffusion limit, we constrain the widths, $\sigma_{d,\delta}$ and $\sigma_{a,\delta}$, to be the same. We constrain the position along the ω_τ axis and the widths of the product peak, $\sigma_{d,\gamma}$ and $\sigma_{a,\gamma}$, to be the same as the preserved bleach peak. As a result, we have four adjustable parameters describing the preserved δ bleach, the positions $\omega_{m,\delta}$ and $\omega_{\tau,\delta}$, the overall width, $\sigma_{d,\gamma} = \sigma_{a,\gamma}$, and the amplitude, A_δ. We have two independently adjustable parameters for the product peak, the shift along the ω_m axis, Δ_w (here Δ_w is not caused by weakening but we use Δ_w to preserve the notation), and the amplitude, A_p. These parameters are summarized in Table I. In Model 4, Δ_w is defined by Eq. (3) (see main text). The position of the product peak along the ω_τ axis is fixed to the position of the preserved δ bleach. The positions and relative amplitudes of the Fermi resonance peaks are determined from the best fit of the $T_w = 125$ fs correlation spectrum. In Model 4, the γ band does not break or weaken hydrogen bonds, so this peak is not included in the calculations.

[1] G. C. Pimentel and A. L. McClellan, *The Hydrogen Bond* (W. H. Freeman, San Francisco, 1960).
[2] J. B. Asbury, T. Steinel, C. Stromberg, S. A. Corcelli, C. P. Lawrence, J. L. Skinner, and M. D. Fayer, J. Phys. Chem. A (to be published).
[3] J. B. Asbury, T. Steinel, C. Stromberg, K. J. Gaffney, I. R. Piletic, A. Goun, and M. D. Fayer, Phys. Rev. Lett. (to be published).
[4] J. B. Asbury, T. Steinel, C. Stromberg, K. J. Gaffney, I. R. Piletic, A. Goun, and M. D. Fayer, Chem. Phys. Lett. **374**, 362 (2003).
[5] K. Gaffney, I. Piletic, and M. D. Fayer, J. Phys. Chem. A **106**, 9428 (2002).
[6] K. J. Gaffney, P. H. Davis, I. R. Piletic, N. E. Levinger, and M. D. Fayer, J. Phys. Chem. A **106**, 12012 (2002).
[7] K. J. Gaffney, I. R. Piletic, and M. D. Fayer, J. Chem. Phys. **118**, 2270 (2003).
[8] I. Piletic, K. Gaffney, and M. D. Fayer, J. Chem. Phys. **119**, 423 (2003).
[9] S. Bratos, G. M. Gale, G. Gallot, F. Hache, N. Lascoux, and J. C. Leicknam, Phys. Rev. E **61**, 5211 (2000).
[10] R. Laenen, G. M. Gale, and N. Lascoux, J. Phys. Chem. A **103**, 10708 (1999).
[11] G. M. Gale, G. Gallot, F. Hache, N. Lascoux, S. Bratos, and J. C. Leicknam, Phys. Rev. Lett. **82**, 1068 (1999).
[12] H. J. Bakker, H. K. Neinhuys, G. Gallot, N. Lascoux, G. M. Gale, J. C. Leicknam, and S. Bratos, J. Chem. Phys. **116**, 2592 (2002).
[13] M. F. Kropman, H.-K. Nienhuys, S. Woutersen, and H. J. Bakker, J. Phys. Chem. A **105**, 4622 (2001).
[14] H.-K. Nienhuys, S. Woutersen, R. A. van Santen, and H. J. Bakker, J. Chem. Phys. **111**, 1494 (1999).
[15] S. Woutersen, U. Emmerichs, and H. J. Bakker, J. Chem. Phys. **107**, 1483 (1997).
[16] R. Laenen, C. Rauscher, and A. Laubereau, J. Phys. Chem. A **101**, 3201 (1997).
[17] H. Graener, T. Q. Ye, and A. Laubereau, J. Chem. Phys. **90**, 3413 (1989).
[18] S. Yeremenko, M. S. Pshenichnikov, and D. A. Wiersma, Chem. Phys. Lett. **369**, 107 (2003).
[19] J. Stenger, D. Madsen, P. Hamm, E. T. J. Nibbering, and T. Elsaesser, J. Phys. Chem. A **106**, 2341 (2002).
[20] J. Stenger, D. Madsen, P. Hamm, E. T. J. Nibbering, and T. Elsaesser, Phys. Rev. Lett. **87**, 027401 (2001).
[21] C. P. Lawrence and J. L. Skinner, J. Chem. Phys. **118**, 264 (2003).
[22] C. P. Lawrence and J. L. Skinner, J. Chem. Phys. **117**, 8847 (2002).
[23] C. P. Lawrence and J. L. Skinner, J. Chem. Phys. **117**, 5827 (2002).
[24] A. Luzar, J. Chem. Phys. **113**, 10663 (2000).
[25] R. Rey, K. B. Møller, and J. T. Hynes, J. Phys. Chem. A **106**, 11993 (2002).
[26] R. Veldhuizen and S. W. de Leeuw, J. Chem. Phys. **105**, 2828 (1996).
[27] A. Staib, J. Chem. Phys. **108**, 4554 (1998).
[28] A. Staib and J. T. Hynes, Chem. Phys. Lett. **204**, 197 (1993).
[29] D. Zimdars, A. Tokmakoff, S. Chen, S. R. Greenfield, M. D. Fayer, T. I. Smith, and H. A. Schwettman, Phys. Rev. Lett. **70**, 2718 (1993).
[30] A. Tokmakoff and M. D. Fayer, J. Chem. Phys. **103**, 2810 (1995).
[31] K. D. Rector, J. R. Engholm, C. W. Rella, J. R. Hill, D. D. Dlott, and M. D. Fayer, J. Phys. Chem. A **103**, 2381 (1999).
[32] P. Hamm, M. Lim, and R. M. Hochstrasser, Phys. Rev. Lett. **81**, 5326 (1998).
[33] M. T. Zanni, M. C. Asplund, and R. M. Hochstrasser, J. Chem. Phys. **114**, 4579 (2001).
[34] K. A. Merchant, D. E. Thompson, and M. D. Fayer, Phys. Rev. Lett. **86**, 3899 (2001).
[35] O. Golonzka, M. Khalil, N. Demirdoven, and A. Tokmakoff, Phys. Rev. Lett. **86**, 2154 (2001).
[36] R. R. Ernst, G. Bodenhausen, and A. Wokaun, *Nuclear Magnetic Resonance in One and Two Dimensions* (Oxford University Press, Oxford, 1987).
[37] M. Khalil, N. Demirdöven, and A. Tokmakoff, J. Phys. Chem. A **107**, 5258 (2003).
[38] M. Khalil, N. Demirdöven, and A. Tokmakoff, Phys. Rev. Lett. **90**, 047401 (2003).
[39] W. Mikenda, J. Mol. Struct. **147**, 1 (1986).
[40] U. Liddel and E. D. Becker, Spectrochim. Acta **10**, 70 (1957).
[41] C. P. Lawrence and J. L. Skinner, Chem. Phys. Lett. **369**, 472 (2003).
[42] S. Woutersen and H. J. Bakker, Phys. Rev. Lett. **83**, 2077 (1999).
[43] K. A. Merchant, D. E. Thompson, Q.-H. Xu, R. B. Williams, R. F. Loring, and M. D. Fayer, Biophys. J. **82**, 3277 (2002).
[44] M. Falk and T. A. Ford, Can. J. Chem. **44**, 1699 (1966).

[45] N. E. Levinger, P. H. Davis, and M. D. Fayer, J. Chem. Phys. **115**, 9352 (2001).
[46] J. E. Bertie and S. L. Zhang, J. Mol. Struct. **413–414**, 333 (1997).
[47] H. Morita and S. Nagakura, J. Mol. Spectrosc. **49**, 401 (1974).
[48] J. E. Bertie and S. L. Zhang, Appl. Spectrosc. **48**, 176 (1994).
[49] S. Mukamel, *Principles of Nonlinear Optical Spectroscopy* (Oxford University Press, New York, 1995).
[50] H. Graener, T. Q. Ye, and A. Laubereau, J. Chem. Phys. **91**, 1043 (1989).
[51] A. Novak, in *Structure and Bonding*, edited by J. D. Dunitz (Springer-Verlag, Berlin, 1974), Vol. 18, pp. 177.
[52] J. B. Asbury, T. Steinel, C. Stromberg, K. J. Gaffney, I. R. Piletic, and M. D. Fayer, J. Phys. Chem. A (to be published).
[53] V. M. Kenkre, A. Tokmakoff, and M. D. Fayer, J. Chem. Phys. **101**, 10618 (1994).
[54] L. K. Iwaki and D. D. Dlott, J. Phys. Chem. A **104**, 9101 (2000).
[55] J. L. Skinner (private communication).